telecom

MDPI

Article

Wearable Flexible Antenna for UWB On-Body and Implant Communications

Mariella Särestöniemi [1,2,*], Marko Sonkki [2], Sami Myllymäki [3] and Carlos Pomalaza-Raez [4]

1 Medical Imaging, Physics and Technology Research Unit, Faculty of Medicine, University of Oulu, 90220 Oulu, Finland
2 Centre for Wireless Communications, Faculty of Information Technology and Electrical Engineering, University of Oulu, 90570 Oulu, Finland; marko.sonkki@gmail.com
3 Microelectronics Research Unit, Faculty of Information Technology and Electrical Engineering, University of Oulu, 90570 Oulu, Finland; sami.myllymaki@oulu.fi
4 Department of Electrical and Computer Engineering, Purdue University, Fort Wayne, IN 46805, USA; cpomalaz@purdue.edu
* Correspondence: mariella.sarestoniemi@oulu.fi; Tel.: +358-40-58-22-935

Abstract: This paper describes the development and evaluation of an on-body flexible antenna designed for an in-body application, as well as on-body communications at ISM and UWB frequency bands. The evaluation is performed via electromagnetic simulations using the Dassault Simulia CST Studio Suite. A planar tissue layer model, as well as a human voxel model from the human abdominal area, are used to study the antenna characteristics next to human tissues. Power flow analysis is presented to understand the power flow on the body surface as well as within the tissues. Simulation results show that this wearable flexible antenna is suitable for in-body communications in the intestinal area, e.g., for capsule endoscopy, in the industrial, scientific, and medical (ISM) band and at lower ultra-wideband (UWB). At higher frequencies, the antenna is suitable for on-body communications as well as in-body communications with lower propagation depth requirements. Additionally, an antenna prototype has been prepared and the antenna performance is verified with several on-body measurements. The measurement results show a good match with the simulation results. The novelty of the proposed antenna is a compact size and the flexible substrate material, which makes it feasible and practical for several different medical diagnosis and monitoring applications.

Keywords: flexible antenna; capsule endoscope; implant communications; in-body propagation; ISM-band; medical monitoring; on-body propagation; UWB

check for updates

Citation: Särestöniemi, M.; Sonkki, M.; Myllymäki, S.; Pomalaza-Raez, C. Wearable Flexible Antenna for UWB On-Body and Implant Communications. *Telecom* **2021**, *2*, 285–301. https://doi.org/10.3390/telecom2030019

Academic Editor: Gino Sorbello

Received: 13 July 2021
Accepted: 31 August 2021
Published: 6 September 2021

Publisher's Note: MDPI stays neutral with regard to jurisdictional claims in published maps and institutional affiliations.

Copyright: © 2021 by the authors. Licensee MDPI, Basel, Switzerland. This article is an open access article distributed under the terms and conditions of the Creative Commons Attribution (CC BY) license (https://creativecommons.org/licenses/by/4.0/).

1. Introduction

Currently, healthcare devices have attracted the interest of many antenna designers [1–4]. The continuous monitoring of a patient can interfere with the freedom of movement, which complicates the use of continuous monitoring. Thus, currently, healthcare systems aim to devise innovative wearable devices for wireless diagnosis, monitoring, and following-up of the patient's health status, involving the motion activity [5]. Among the technological devices currently in a clinical use, we can find several wearable antennas implemented in those systems. Such antennas are mounted on the patient by means of attachment belts and the communication is established wirelessly with internal or external devices with respect to the human body [6–8]. To ensure good performance and safety of these connected devices, many issues should be taken into the account during the design stage [9–11]. The antenna radiating properties close to a human body should be investigated, as well as the antenna on-body matching at different body locations.

The design of new, sophisticated antennas for different body area applications has been an active research topic for several years [12–25]. Recently, there has been recognized a need for especially flexible, wearable antennas for biomedical applications. A couple

of recently published surveys on flexible antennas and their materials [26–28] give a comprehensive overview on the previously published flexible antennas having different sizes, shapes, materials, properties, and their intended uses. One can find several flexible antennas designed especially for industrial, scientific, and medical (ISM) bands or ultra-wideband (UWB) [29–55]. However, published studies for flexible on-body antennas have emphasized on-body communications, leaving aside the implant communications. Only a few initial flexible antenna studies have been presented for the in-body applications: for tumor detection [52–54], brain hemorrhage detection [35], or in general head imaging [36]. These proposed antennas operate at least partially on UWB band or ISM band. In general, a very limited number of flexible antenna studies can be found covering the whole UWB band as well as ISM band 2.45 GHz.

When considering practical applications, the size of the antenna is crucial. Several wearable flexible antennas covering ISM bands 2.45 GHz or lower UWB bands are approximately at least 30 mm on the shorter side and even 50 mm on the longer side [26]. Antenna total efficiency, which is a ratio of the power delivered to the antenna relative to the power radiated from the antenna, is usually rather low with flexible antennas at UWB frequencies, approximately −20 dB [51], since the antenna operates less efficiently in proximity to the human body. The closer the antenna is to the skin surface, the weaker the total efficiency.

To the authors' best knowledge, wearable flexible antennas for in-body communications for the entire UWB band, as well as ISM bands, have not yet been reported. This paper addresses this uncovered issue in flexible antenna design for medical monitoring and diagnosis applications by presenting for the first time in-body propagation results with the wearable flexible antenna. As an example case, the suitability of this flexible antenna for implant communications and gastrointestinal track monitoring, e.g., for wireless capsule endoscopy (WCE), is studied by evaluating frequency domain radio channel characteristics between this antenna and a UWB capsule endoscope antenna. Furthermore, the antenna is shown to be feasible for on-body communications as well.

The study is carried out using electromagnetic simulations as well as measurements with a hand phantom and a volunteer. Simulations are conducted with Dassault Simulia CST Studio Suite [55] using an abdominal tissue layer model as well as the torso anatomical voxel model's torso from the abdominal area. The power flow analysis is conducted to evaluate propagation depth at different frequencies in the abdominal tissues. Specific absorption ratio (SAR) values, total antenna efficiency, and impact of the bending is studies, while simulation and measured results are also compared.

This is the first flexible on-body antenna that has been presented for implant communications and which covers such a wide frequency band. Besides, compared to the recently published antenna structures, the proposed monopole antenna is a very simple, more compact in size, and represents good peak efficiency.

This paper is organized as follows. Section 2 presents the antenna model and prototype. Section 3 presents the methodology, including a description of the layer model and the voxel model used in this study. This section also discusses pros and cons of these simulation models. Additionally, a description of measurements is given. Section 4 presents the simulation and measurement results. Section 4 presents a discussion, including future perspectives.

2. Antenna Model and Prototype

The novelty of the proposed antenna is the compact size with the use of a flexible substrate material, which is suitable for in-body and on-body communications. The antenna structure is illustrated in Figure 1a. The prototype of the antenna is presented in Figure 1b. The antenna is printed on the front side of the flexible Rogers XT8100 substrate, having the following dimensions: width 20 mm, height 30 mm, and 50 µm of substrate thickness.

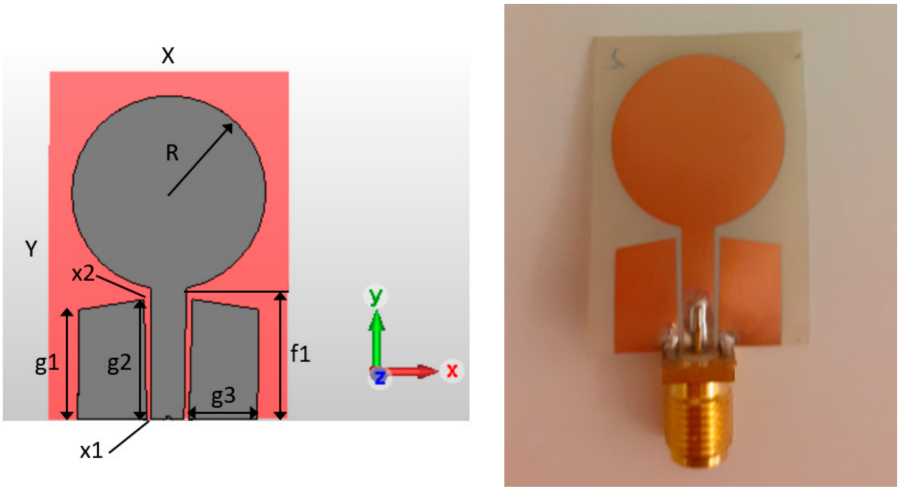

(**a**) (**b**)

Figure 1. Flexible antenna (**a**) simulation model, (**b**) prototype.

The antenna dimensions are summarized in Table 1 as follows: R is the radius of the monopole, f1 is the total length of the feed line, g1 is the height of the shorter edge of the monopole ground, g2 is the height of the longer edge of the monopole ground, g3 is the width of the monopole ground, x1 is the lower gap of the coplanar feed, and x2 the higher gap of the coplanar feed.

Table 1. Dimensions of the antenna structure.

Parameter	X	Y	R	f1	g1	g2	g3	x1	x2
Dimension [mm]	20	30	8.1	11	9.1	10	5.7	0.4	0.6

3. Methodology

The novel antenna is evaluated with (1) electromagnetic simulations and (2) measurements using the prototype of the antenna. These methodologies are described in the following subsections.

3.1. Simulations

The antenna is designed and its performance is evaluated using Dassault Simulia CST Studio suite software [55], which is based on finite integration technique (FIT) [56]. Since the antenna is designed to operate tightly attached on the human skin, the performance is evaluated using two human tissue models, namely (a) a planar tissue layer model, and (b) CST's anatomical voxel model Laura, which are presented in Figure 2a,b, respectively.

The thicknesses of the different tissue layers in the planar model are presented in Table 2, where also the relative permittivity of the tissues (ϵ_r) and wavelength (λ) in the tissues are presented at the selected frequencies [57]. As can be seen, the relative permittivity and wavelength varies significantly from tissue to tissue, which has a clear impact on the propagation characteristics, as will be described through the paper. Figure 2b presents the torso of Laura voxel model used in the simulations. Laura voxel resembles a young, lean female. Only the part of the voxel model's abdomen area is included in the simulations to save simulation time. The pixel resolution of the Laura voxel is $1.88 \times 1.88 \times 1.25$ mm^3.

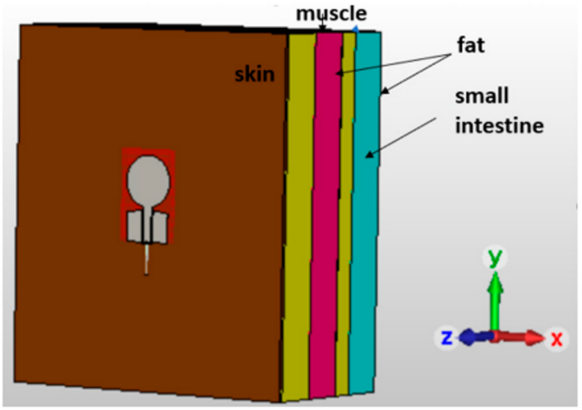

(**a**)

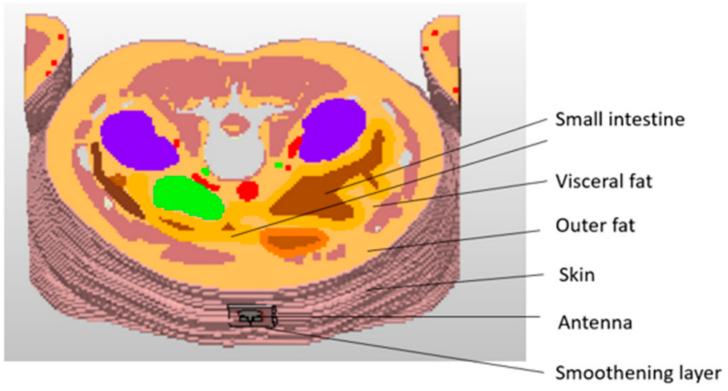

(**b**)

Figure 2. (**a**) Tissue layer model, (**b**) CST's anatomical voxel model Laura.

Table 2. Thicknesses of the tissue layers, relative permittivity (ϵ_r) of tissue and wavelength in the tissue (λ) at different frequencies.

Tissue (Thickness)	**Relative Permitivity ϵ_r/Wavelength λ [m] at Selected Frequencies**					
	Frequency [GHz]					
	2.45	**3.1**	**5.8**	**7**	**9**	**10.6**
Skin (1.4 mm)	38.0/0.022	37.4/0.015	35.1/0.009	33.1/0.42	32.0/0.42	30.7/0.005
Fat (outer:15 mm, inner 7.5 mm)	5.28/0.053	5.21/0.04	4.95/0.023	4.84/0.20	4.68/0.015	4.58/0.013
Muscle (15.13 mm)	55.0/0.04	51.9/0.013	48.5/0.072	46.8/0.006	44.12/0.05	42.0/0.0042
Small intestine (15 mm)	59.4/004	53.8/0.013	48.5/00.07	46.7/0.006	43.6/0.049	41.2/0.0042

The layered tissue models and voxel models have their own advantages and disadvantages in the evaluations as described, e.g., in [58]. The layered tissue model provides possibility to verify antenna performance and radio channel characteristics with a lower complexity. Additionally, the thickness of the tissue layers is easy to vary in the simple layer models. However, the deficiency of the layer model is the simplicity, especially in the in-body propagation studies: it cannot exploit multipath rich in-body propagation environment similar to the realistic human voxel models, in which the tissue thicknesses and thickness variations are designed according to a real human body. With anatomical voxel models, more realistic performances can be obtained. For instance, in the capsule endoscopy evaluations, it is crucial to use the realistic models since the abdominal muscles have certain shape with clear thickness variation. The areas with thinner/none muscle

layer, e.g., in the central line of the abdomen, can provide "easier" propagation paths for the signal since the signal can avoid traveling through the muscle layer which has high propagation loss [59]. With layer modes, such realistic evaluations are not possible. Besides, fat as a propagation channel can be studied more efficiently with the voxel models [59]. Deficiency of the voxel models is the pixelization as well as higher computational complexity. The higher the resolution, i.e., the smaller the pixel size in the voxel model, the higher the complexity. Besides, in some cases, pixelization may cause challenges in the modeling, e.g., in the cases when the antenna is supposed to be tightly attached in the human skin. Such cases may require the use of smoothening layers, which consist of thin skin and fat layers inserted to the voxel model just below the on-body antenna to compensate non-smoothness due to pixelization as described, e.g., in [60].

The proposed flexible antenna has been designed to operate as tightly attached to the skin. Thus, some modifications have to be made for the voxel models with pixels to ensure smooth contact with the voxel's skin surface. Although the pixels of the Laura-voxel are relatively small due to high resolution, they still cause air gaps between the antenna and the skin as shown in Figure 3a. The air gaps decrease matching of the antennas and thus, require the use of smoothening layers, as shown in Figure 3b. In realistic situations, the on-body antenna is tightly attached on the skin. Due to this "smoothening layer", the model is more realistic as tight attachment of the antenna on the skin is achieved.

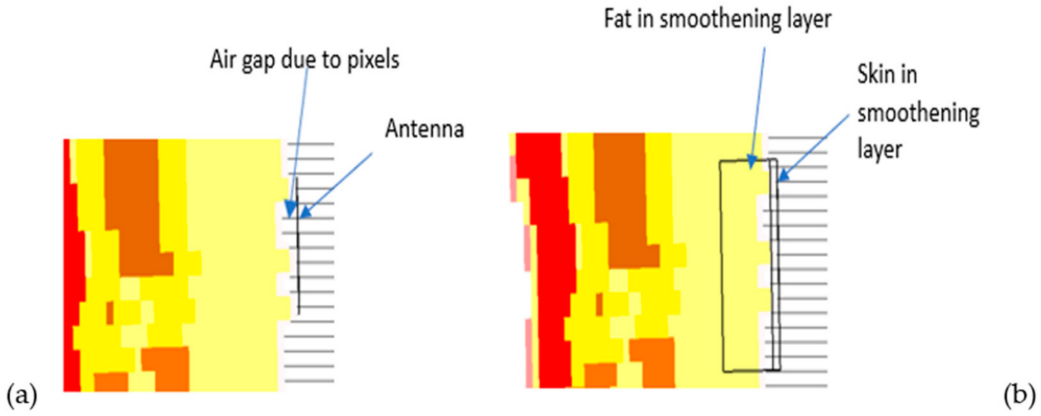

Figure 3. (**a**) Vertical cross-cut illustrating the air gaps between the skin and the antenna due to pixels of the voxel model, (**b**) Smoothening layer replacing air gaps.

3.2. Measurements

Simulation results are verified with an antenna prototype produced based on the simulation model. Antenna reflection coefficient measurements were conducted using an Agilent Vector Network Analyzer 8720ES, with the SOLT-calibration for the frequency range of 2–11 GHz with 50-ohm coaxial cables, and with an input reference power of 5 dBm. The antenna's efficiency was measured with Satimo Starlab antenna measurement system and with SH2000 dual ridge antenna.

A hand phantom of IXB-090 provided by IndexSAR company was used in the measurements. The phantom hand was vertically oriented along the X-axis in the Satimo coordination system, and the antenna was located on top of the hand on XY-plane and approximately on 1 mm distance to the surface of the hand. The feed cable was installed in the Z-axis direction connected to the 90-degree turn connector, and finally the antenna, where the antenna connector was pointing to +Y-axis direction and the antenna open end to the Y-axis direction, as presented in Figure 4, where the 90 degree turn connector was mechanically supported by the paper tape. The total antenna efficiency was measured both in the free space and on the hand. Moreover, the S11 parameter of the antenna was measured with a female volunteer on the hand area as well as on the abdomen area. The Ethical

Committee of the Human Sciences of University of Oulu has granted approval for the antenna measurements on the human abdomen area with the permission number 14/2018.

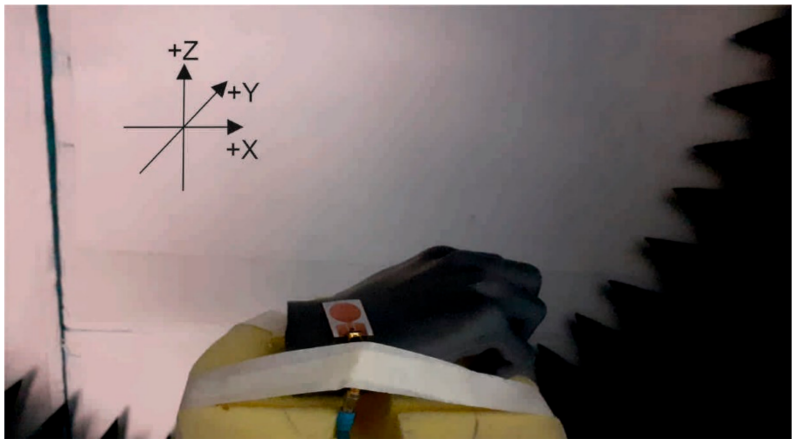

Figure 4. Flexible antenna on the hand phantom in Satimo.

4. Results

This section presents simulation and measurement-based evaluations of the flexible antenna. Firstly, the antenna matching is studied in Section 4.1 by evaluating S11 parameter as the antenna is fed with discrete port and with coaxial cables having different thicknesses. Then, in Section 4.2, the measured antenna matching is evaluated in different body parts, located directly on the skin or above the cloth of the volunteer. Additionally, impact of the bending is studied with measurements. Section 4.3 compares the simulated and measured S11 parameters as well as antenna efficiencies. In Sections 4.4 and 4.5, the antenna's usability for in-body and on-body communications at different frequencies is evaluated by studying power flow representations with the layer model as well as the voxel model. Channel characteristics between the flexible antenna and a UWB capsule endoscope model is evaluated in Section 4.6. Finally, the antenna's safety is studied by SAR evaluations in Section 4.7.

4.1. Simulated S11 Parameters

In this subsection, the impact of the antenna feeding as well as the impact of the antenna-skin distance (a-s) for S11 parameter is studied with the layer model. Discrete port as well as coaxial cables with thicknesses 6.5 mm and 1 mm are used in the simulations. With discrete port, the antenna can be attached directly on the skin layer in the simulations. Thickness of the coaxial cable determines the antenna-skin distance in the simulation model, as seen in Figure 5a. With the coaxial cable thickness of 6.5 mm, the antenna-skin distance is 3.2 mm, whereas with the coaxial cable thickness 1 mm, the antenna-skin distance is 0.94 mm. Furthermore, we evaluate a case whereby we set the antenna with 1 mm coaxial cable directly located on the skin layer so that the skin layer is partially cut below the coaxial cable to enable direct contact between the skin and the antenna, as shown in Figure 5b.

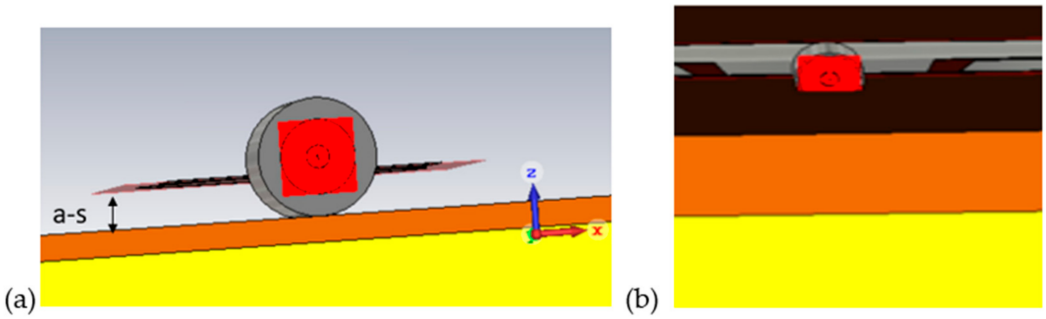

Figure 5. Dependence of the antenna-skin (a-s) distance from the cable length: (**a**) a-s = 3.2 mm as the cable thickness is 6.5 mm, (**b**) a-s = 0 mm as the antenna is on the skin layer which has been cut partially below the thin cable.

Figure 6 presents the S11 results obtained with these different cases. As observed, the feeding and the antenna-skin distance has clear impact on the S11 results. The closer the antenna is to the skin, the better the antenna matching obtained for the whole frequency range 2–11 GHz. This result is positive since the wearable flexible antenna is targeted to work directly on the skin contact. The best matching is obtained with the discrete port.

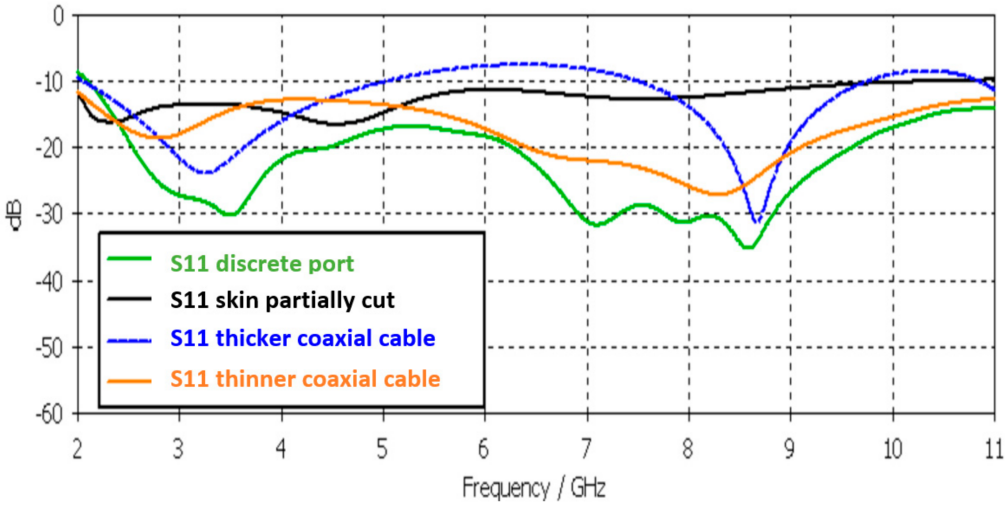

Figure 6. S11 results simulated with the layer model with different antenna-skin distances (coaxial cable thicknesses).

4.2. Measured S11 Parameters

In this subsection, we evaluate S11 parameters by antenna prototype measurements. The antenna is measured on the abdomen and on the hand, as shown in Figure 7a,b, respectively. The measurements were taken with and without the thin cloth between the antenna and the skin. The thickness of the cloth was approximately 3 mm. The measured S11 results in these different cases are shown in Figure 8. Additionally, S11 results measured with the hand phantom are included in the figure.

It is observed that in the measurements, the antenna matching is relatively good within the whole bandwidth. One can note the variation between the measured S11 results. The best antenna matching is obtained as the antenna is located directly on the skin of the abdomen. The S11 parameter remains below −10 dB up to 9 GHz, after which it remains below −9 dB. As the antenna is located on the hand, directly on the skin, the S11 parameter remains below −10 dB within the whole measured range except at 2–3.7 GHz and 6.5–7 GHz, in which the S11 remains below 8 dB. Including the cloth between the antenna and the skin decreases antenna matching slightly at the frequency range 6–7 GHz, but interestingly improves antenna matching at lower frequencies.

Figure 7. (**a**) Antenna located on the hand, (**b**) antenna located on the abdomen, both locations measured with and without the thin cloth between the antenna and the skin.

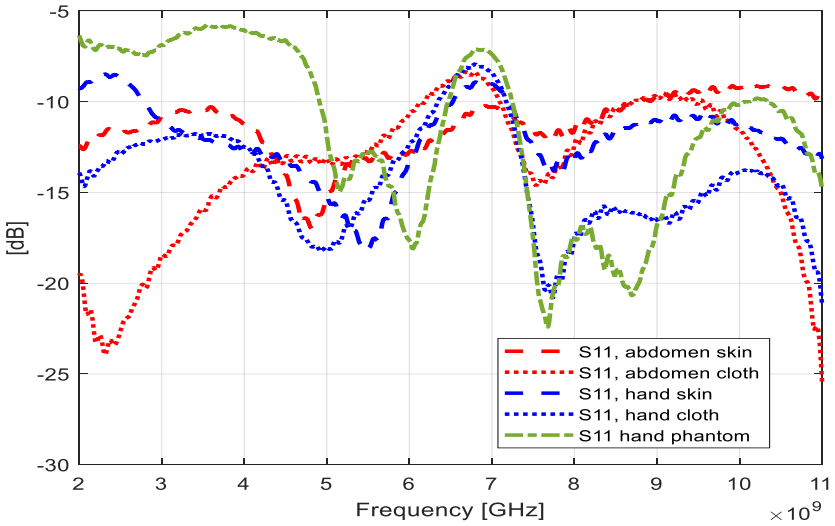

Figure 8. Measured S11 in different cases: antenna set on the hand phantom (green line), on the volunteer's hand with and without the cloth between the antenna and the skin (blue lines), volunteers abdomen with and without the cloth between the antenna and the skin (red lines).

Next, the impact of bending the antenna on S11 results is studied on the hand and on the abdomen by locating the antenna on the areas where occurs natural bending, e.g., on side of the hand. The measurements were taken with and without the cloth between the antenna and the skin. The results are shown in Figure 9. The S11 values measured on the unbended, i.e., straight part, are included for comparison. It is observed that the bending causes some changes in S11s at certain frequencies: on the hand, the major changes can be seen below 4.5 GHz, and on the abdomen, major changes are seen above 9.5 GHz. However, the antenna matching remains good, despite bending. In fact, the bending even improved the antenna matching on the abdomen measurements.

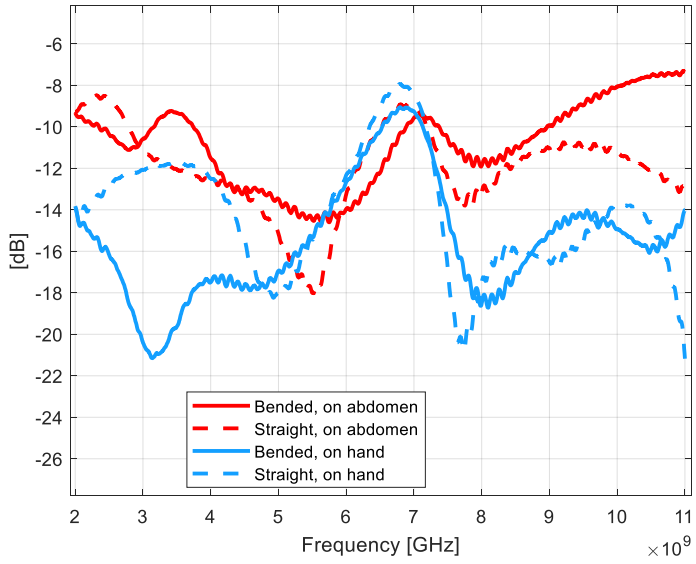

Figure 9. Impact of the bending of the antenna, measured on the abdomen (blue curves) and on the hand (red curves).

4.3. Comparison of Simulated and Measured Results for S11 Parameter and Antenna's Total Efficiency

This subsection compares the simulated and measured S11 results. Figure 10 presents the simulated S11 result (in which the antenna is fully attached on the skin layer surface) as well as S11 parameters measured on the abdomen and skin with cloth. It is noted that a similar tendency can be found in simulated and measured results. There are some fluctuations along the evaluated frequency range. At certain frequencies, simulated and measured S11 parameters match better than in others. However, the differences are moderate and antenna matching is good in both simulated and measurement cases.

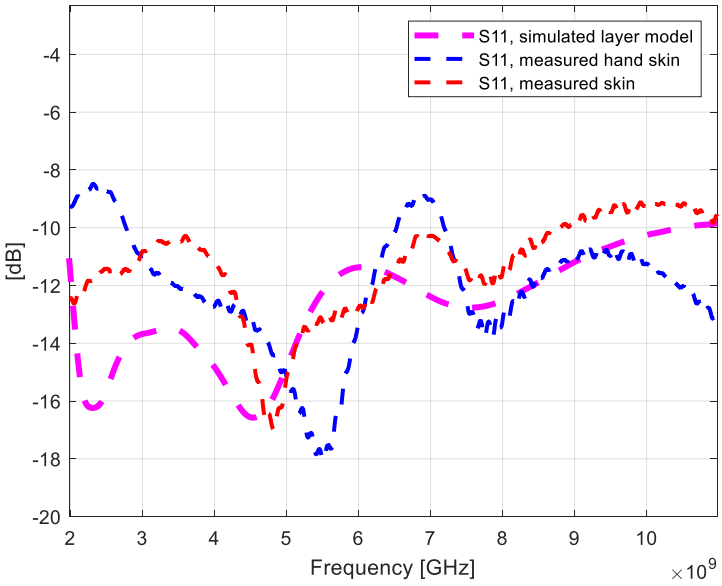

Figure 10. Comparison of the S11 parameters obtained by layer model simulations and measurements on the hand (with and without the cloth).

Next the antenna total efficiencies are studied by simulations and measurements. In the simulations, total efficiencies are measured in the cases when the thicker cable is used (antenna skin distance is 3.2 mm) as well as in the case when the antenna is fully attached

on the skin (skin partially cut below the thinnest cable). The measured efficiency is obtained when the antenna is on the hand phantom. The simulated and measured efficiencies at different frequencies are summarized in Table 3. The efficiency results obtained from simulations, in which the antenna is fully attached on the skin layer, correspond well with the hand phantom measurements at lower frequencies. At higher frequencies the difference is several decibels. This is assumed to be due to the hand phantom properties. The hand phantom is designed for a lower UWB band, and thus the results obtained at higher UWB range are less reliable. In the simulations, as the antenna–skin distance increases, the efficiency improves slightly.

Table 3. Measured and simulated total efficiencies at different antenna-skin distances.

Frequency [GHz]	**2.45**	**3.1**	**4.0**	**5.8**	**7.0**	**9.0**	**10.6**
Simulated, a-s = 0 mm [dB]	−15.5	−16.5	−17.2	−17.1	−16.0	−17.0	−17.5
Simulated, a-s = 3.2 mm [dB]	−10.5	−12.5	−11.0	−7.5	−7.0	−4.2	−4.5
Measured [dB]	−16.6	−14.8	−11.0	−6.5	−7.1	−5.9	−6.1

4.4. Power Flow Analysis at Different Frequencies for Layer Model

Next, we study in-body propagation from the proposed flexible antenna at the selected frequencies using the notion of power flow. Power flow represents the directional energy flux (the energy transfer per unit area per unit time) of an electromagnetic field. The total electromagnetic power flowing through a given surface is represented by the flux of the Poynting vector through it. In this case, the power flow values are selected to be expressed as decibels. Power flow values are normalized so that 0 dB is the maximum, which means the value at the transmitting antenna. The plotted dB range is −65–0 dB which is chosen to illustrate coverage according to the receiver's sensitivity, 65 dB [60].

Figure 11a–g presents the power flow variation from the flexible antenna (ranging from 0 to −65 dB) on a 2D vertical cross-cut plane of the tissue layer model at 2.45, 3.1, 4.1, 5.8, 7, 9, and 10.6 GHz, respectively. All these frequency ranges are presented to enable a comparison in the power flow and especially in the propagation depth at different frequency ranges targeted for medical communications.

As is noted, the small intestine layer is reached easily up to a frequency of 3.1 GHz since the propagation loss is more moderate at lower frequencies. However, as the frequency increases, power loss increases affecting straightly to the propagation depth. The outer corner of the small intestine layer with the selected layer model thicknesses can be achieved up to 7 GHz, but at 9 GHz the small intestine area is not reachable. However, at the higher frequencies the flexible antenna could be used for the applications where the requirements for the propagation depth are minor. Next, the simulated power flows are studied with the voxel models.

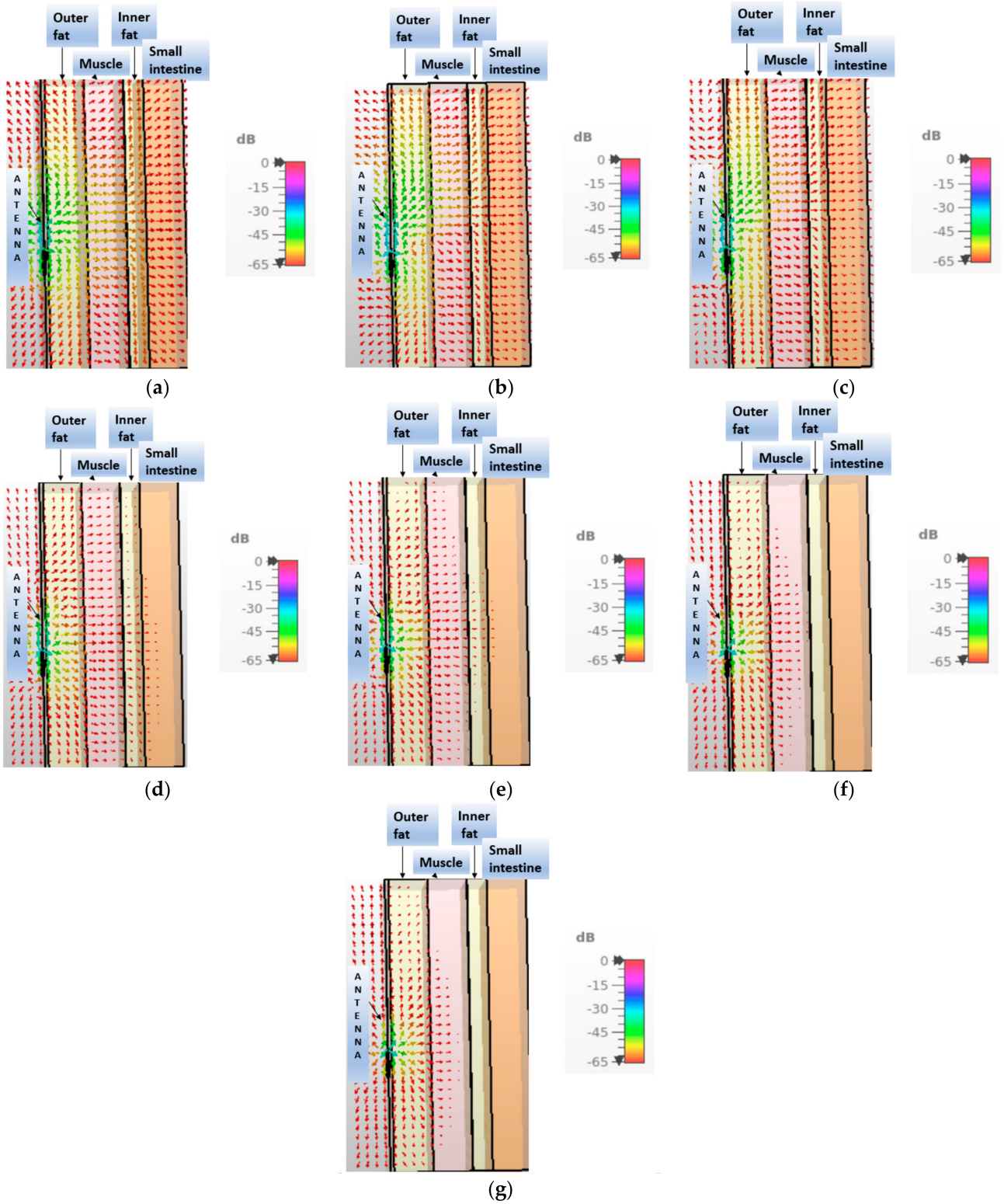

Figure 11. Power flows in the vertical cross-cuts of the layer models at (**a**) 2.45 GHz, (**b**) 3.1 GHz, (**c**) 4 GHz, (**d**) 5.8 GHz, (**e**) 7 GHz, (**f**) 9 GHz, and (**g**) 10.6 GHz for dB range −65–0 dB.

4.5. Power Flow Analysis at Different Frequencies for Voxel Models

This subsection presents power flow evaluations obtained with an anatomical voxel model with flexible antenna set above the navel. Both in-body and on-body propagation

evaluations are more realistic with voxel models than with layer models due to more realistic shape and anatomical structure of the voxel models. Due to significantly higher computational complexity of voxel models, in this case, we evaluate power flows only up to 5.8 GHz. Figure 12a–d presents power flow at 2.45, 3, 4, and 5.8 GHz, respectively. Further, in this case, the plotted dB range is −65–0 dB. At this horizontal cross-cut, the front part of the small intestine area is fully covered if the ISM frequency band of 2.45 GHz is used. Only the outer rightmost corner of the small intestine area is outside of this dB range. However, with multiple on-body antennas, the whole small intestine area would be easily covered. As the frequency increases, power flow coverage decreases. However, even at 5.8 GHz, the small intestine is achieved right below the antenna.

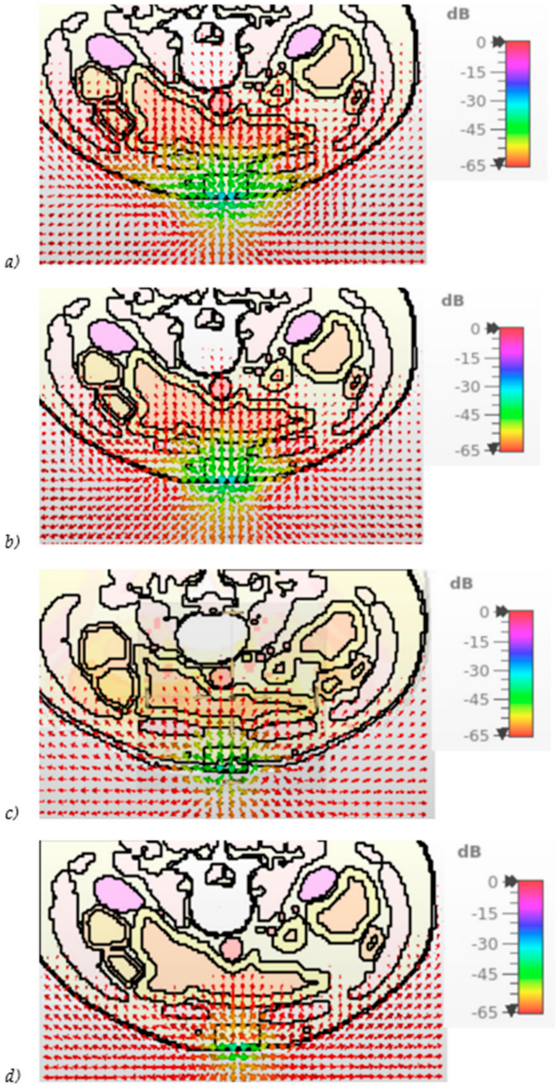

Figure 12. Power flows in the vertical cross-cuts of the voxel models at (**a**) 2.45 GHz, (**b**) 3.1 GHz, (**c**) 4 GHz, (**d**) 5.8 GHz, for the dB range −65–0 dB.

The presented flexible antenna is suitable also for on-body communications since the signal from the on-body antenna travels widely also via body surface. At higher frequencies, the propagation depth decreases clearly, but coverage on the body surface remains almost at the same level at this horizontal cross-cut.

4.6. Channel Evaluations between the Flexible Antenna and UWB Capsule Endoscope Model

Finally, the usability of the proposed flexible antenna for capsule endoscopy is studied by evaluating the channel characteristics between the flexible antenna and an UWB capsule endoscope model. The UWB capsule antenna is illustrated in Figure 13a and was originally presented in [25]. Figure 13b presents the dimensions of the capsule model used in the simulations.

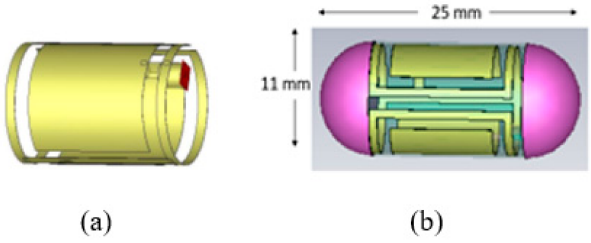

Figure 13. (**a**) UWB capsule antenna, (**b**) UWB capsule endoscope model.

In the simulation, the layer model described in Section 2 is used. The capsule model is set inside the small intestine layer in the same line as the flexible antenna. The simulations were carried out only until 7 GHz, since the power loss was expected to be excessively high after 7 GHz based on power flow results.

The frequency domain channel characteristics, i.e., the channel parameter S21, is presented in Figure 14. As expected, the S21 parameter decreases smoothly as the frequency increases. In this case, the signal from the capsule could be detected easily up to 5.4 GHz until which point the channel strength remains above −65 dB. Evidently, the receivers with better sensitivity, e.g., −85 dB as stated in [60], could detect the signal even at 7 GHz.

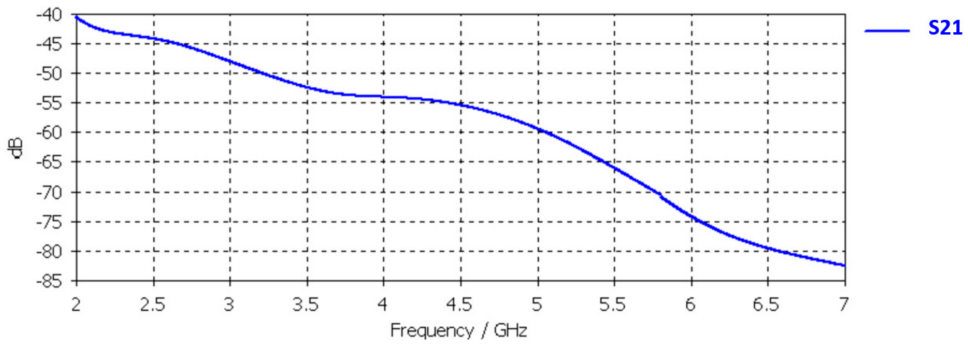

Figure 14. S21 channel parameter between the flexible antenna and UWB capsule.

4.7. SAR Evaluations

SAR is a measure of the rate at which energy is absorbed per unit mass by a human body when exposed by electromagnetic field. According to IEEEC95.3 standard, the allowed SAR value is 2 W/kg [10]. The safety of the proposed antenna structure is evaluated by CST's SAR calculations. The evaluations are carried out with the simulation model case shown in Figure 5b, in which the antenna–skin distance is 0 mm. An input power of 5 dBm was used in the SAR evaluations since it is the same power as was used in the measurements. With this input power, the maximum SAR value (10 g) is calculated for the selected frequency ranges, and these are summarized in Table 4. The maximum SAR values vary from 0.027 (2.45 GHz) to 0.053 (10.6 GHz), which are clearly below the standardized limit. Hence, this antenna can be considered safe for in- and on-body communications.

Table 4. Simulated SAR-values at different frequencies as the input power is 5 dBm.

Frequency [GHz]	**2.4**	**3.1**	**4.0**	**5.8**	**7.0**	**9.0**	**10.6**
SAR	0.027	0.032	0.040	0.046	0.050	0.052	0.053

5. Discussion

This paper presents a compact-sized wearable flexible monopole antenna designed for in-body and on-body communications at ISM and UWB frequency bands. Compared to the recently published wearable flexible antennas structures, the proposed monopole antenna is a very simple, more compact in size, and represents good radiation performance in terms of total efficiency. Additionally, this is the very first flexible antenna paper presenting evaluations for in-body communications by studying radio channel characteristics between the proposed antenna and an UWB capsule endoscope with simulations.

The antenna evaluations were performed via electromagnetic simulations using CST Studio Suite simulation software, utilizing a tissue layer model for the abdominal tissues as well as an anatomical voxel model. Additionally, the antenna prototype was prepared, and measurements were carried out with a hand phantom as well as with a volunteer.

It was found that this antenna operates well both in ISM and UWB bands. The closer the antenna is to the skin surface, the better the antenna matching. This is an important characteristic for flexible antennas designed for body area networks and it also provides potential for many different applications.

Another important characteristic is that the bending of the antenna has only minor effect on the S11 results since the antenna would naturally bend when attached on the human skin. The power flow analysis show that the propagation depth in the abdominal tissue layer model and voxel model is good up to 5.8 GHz. Besides, the channel evaluations between the flexible antenna and a UWB capsule model using the layer model are in line with the power flow results. With the proposed flexible antenna, the signal could be detected easily up to 5.8 GHz if the receiver's sensitivity limit is around −65 dBm [61]. With receivers having better sensitivity [62], even the signals transmitted at 7 GHz could be detected smoothly in this case. Naturally, as the propagation depth increases, also power loss increases and thus, 7 GHz frequency will become excessive to detect signals from the capsule which is deep inside the intestine area especially with persons having thicker muscle and fat layers. Overall, the presented results indicate that this flexible antenna would operate well as an on-body antenna in the capsule endoscopy if lower frequencies as well as multiple receiving antennas are used. At higher frequencies, the antenna is suitable for on-body communications as well as for in-body communications with lower propagation depth requirements.

The properties of the capsule endoscope antenna also have a strong impact on the radio channel evaluations between the on-body antenna and the implant antenna, especially in the practical scenarios where the capsule can rotate inside the intestine. Being in arbitrary position, the channel attenuation may become excessively high in unfavorable capsule positions if both on-body and implant antennas are linearly polarized. Hence, the use of circularly polarized efficient implant antennas, as presented, e.g., in [13–15], could significantly improve the channel condition in certain capsule positions. Additionally, enhancement of the power transmission link in the implant communications requiring deep propagation depths, as presented in [14], could also improve the performance of implant communications in practical scenarios.

As a future work, we will evaluate radio channel characteristics between the flexible antenna and a capsule endoscope model with simulations using several different anatomical voxel models having different sizes and body constitutions. Additionally, we will verify the simulation results measuring human tissue mimicking phantoms as well as pork tissue. Besides, our future work will include evaluations of the antenna's usability for different medical monitoring and diagnostic applications in different body parts. We also aim to use more efficient and circularly polarized implant antennas for realistic evaluations.

Author Contributions: Conceptualization, M.S. (Marko Sonkki), S.M., M.S. (Mariella Särestöniemi) and C.P.-R.; methodology, M.S. (Mariella Särestöniemi), S.M. and M.S. (Marko Sonkki); software M.S. (Mariella Särestöniemi); validation, M.S. (Mariella Särestöniemi), S.M. and M.S. (Marko Sonkki); formal analysis, M.S. (Mariella Särestöniemi), S.M. and M.S. (Marko Sonkki); investigation M.S. (Marko Sonkki), M.S. (Mariella Särestöniemi) and S.M.; data curation, M.S. (Mariella Särestöniemi), S.M.; writing—original draft preparation, M.S. (Mariella Särestöniemi), S.M., M.S. (Marko Sonkki) and C.P.-R.; writing—review and editing, M.S. (Mariella Särestöniemi), S.M., M.S. (Marko Sonkki) and C.P.-R.; visualization, M.S. (Mariella Särestöniemi); supervision, M.S. (Marko Sonkki) (also original antenna design) and C.P.-R. All authors have read and agreed to the published version of the manuscript.

Funding: This research was partially funded by Centre for Wireless Communications, University of Oulu, and supported by Academy of Finland 6Genesis Flagship (grant 318927), with the European Union Horizon 2020 programme under the Marie Sklodowska-Curie grant agreement (No. 872752).

Institutional Review Board Statement: The Ethical Committee of the Human Sciences of University of Oulu has granted approval for the antenna measurements on the human abdomen area with the permission number 14/2018.

Informed Consent Statement: Not applicable.

Data Availability Statement: The data presented in this study are available on request from the corresponding author.

Acknowledgments: ExcellAnt is acknowledged for UWB capsule antenna's redesign.

Conflicts of Interest: The authors declare no conflict of interest.

References

1. Paolini, G.; Masotti, D.; Antoniazzi, F.; Cinotti, T.S.; Costanzo, A. Fall Detection and 3-D Indoor Localization by a Custom RFID Reader Embedded in a Smart e-Health Platform. *IEEE Trans. Microw. Theory Tech.* **2019**, *67*, 5329–5339. [CrossRef]
2. Xu, L.-J.; Duan, Z. Differentially fed metal frame antenna with common mode suppression for biomedical smartband appli-cations. *Radio Sci.* **2018**, *53*, 485–495. [CrossRef]
3. Li, Y.; Zhang, M. Study on a Cylindrical Sensor Network for Intelligent Health Monitoring and Prognosis. *IEEE Access* **2018**, *6*, 69195–69202. [CrossRef]
4. Srivastava, A.; Sankar, N.K.; Chatterjee, B.; Das, D.; Ahmad, M.; Kukkundoor, R.K.; Saraf, V.; Ananthapadmanabhan, J.; Sharma, D.K.; Baghini, M.S. Bio-WiTel: A Low-Power Integrated Wireless Telemetry System for Healthcare Applications in 401–406 MHz Band of MedRadio Spectrum. *IEEE J. Biomed. Health Inform.* **2018**, *22*, 483–494. [CrossRef] [PubMed]
5. Wang, C.; Chen, S.; Yang, Y.; Hu, F.; Liu, F.; Wu, J. Literature review on wireless sensing-Wi-Fi signal-based recognition of human activities. *Tsinghua Sci. Technol.* **2018**, *23*, 203–222. [CrossRef]
6. Bresnahan, D.; Li, Y. Investigation of Creeping Wave Propagation Around the Human Head at ISM Frequencies. *IEEE Antennas Wirel. Propag. Lett.* **2017**, *16*, 2767–2770. [CrossRef]
7. Teshome, A.K.; Kibret, B.; Lai, D.T.H. A Review of Implant Communication Technology in WBAN: Progress and Challenges. *IEEE Rev. Biomed. Eng.* **2018**, *12*, 88–99. [CrossRef] [PubMed]
8. Haghi, M.; Stoll, R.; Thurow, K. Pervasive and Personalized Ambient Parameters Monitoring: A Wearable, Modular, and Configurable Watch. *IEEE Access* **2019**, *7*, 20126–20143. [CrossRef]
9. Ahmed, G.; Islam, S.U.; Shahid, M.; Akhunzada, A.; Jabbar, S.; Khan, M.K.; Riaz, M.; Han, K.J. Rigorous Analysis and Evaluation of Specific Absorption Rate (SAR) for Mobile Multimedia Healthcare. *IEEE Access* **2018**, *6*, 29602–29610. [CrossRef]
10. IEEE Standard for Safety Levels with Respect to Human Exposure to Electric, Magnetic, and Electromagnetic Fields, 0 Hz to 300 GHz. *In IEEE Std C95.1-2019 (Revision of IEEE Std C95.1-2005/ Incorporates IEEE Std C95.1-2019/Cor 1-2019)*. 4 October 2019, pp. 1–312. Available online: https://ieeexplore.ieee.org/document/8859679 (accessed on 30 August 2021).
11. Federal Communications Commission (FCC). Medical Device Radiocommunications Service (MedRadio). 47 C.F.R, Part 95. Available online: https://www.fcc.gov/medical-device-radiocommunications-service-medradio (accessed on 8 January 2021).
12. Dumanli, S. A digitally assisted repeater antenna for implant communications. In Proceedings of the 2017 11th European Conference on Antennas and Propagation (EUCAP), Paris, France, 19–24 March 2017; pp. 181–184.
13. Kaim, V.; Kanaujia, B.K.; Kumar, S.; Choi, H.C.; Kim, K.W.; Rambabu, K. Ultra-Miniature Circularly Polarized CPW-Fed Implantable Antenna Design and its Validation for Biotelemetry Applications. *Sci. Rep.* **2020**, *10*, 1–16. [CrossRef]
14. Ding, S.; Koulouridis, S.; Pichon, L. Implantable Wireless Transmission Rectenna System for Biomedical Wireless Applications. *IEEE Access* **2020**, *8*, 195551–195558. [CrossRef]
15. Magill, M.K.; Conway, G.A.; Scanlon, W.G. Circularly Polarized Dual-Mode Wearable Implant Repeater Antenna with Enhanced Into-Body Gain. *IEEE Trans. Antennas Propag.* **2020**, *68*, 3515–3524. [CrossRef]

16. Iqbal, A.; Basir, A.; Smida, A.; Khaddaj Mallat, N.; Elfergani, I.; Rodriguez, J.; Kim, S. Electromagnetic Bandgap Backed Millimeter-Wave MIMO Antenna for Wearable Applications. *Access IEEE* **2019**, *7*, 111135–111144. [CrossRef]
17. Kanagasabai, M.; Sambandam, P.; Alsath, M.G.N.; Palaniswamy, S.; Ravichandran, A.; Girinathan, C. Miniaturized Circularly Polarized UWB Antenna for Body Centric Communication. *IEEE Trans. Antennas Propag.* **2021**, 1–8. [CrossRef]
18. Tak, J.; Woo, S.; Kwon, J.; Choi, J. Dual-Band Dual-Mode Patch Antenna for On-/Off-Body WBAN Communications. *IEEE Antennas Wirel. Propag. Lett.* **2015**, *15*, 348–351. [CrossRef]
19. Kissi, C.; Sarestoniemi, M.; Kumpuniemi, T.; Sonkki, M.; Myllymaki, S.; Srifi, M.N.; Pomalaza-Raez, C. Directive Low-Band UWB Antenna for In-body Medical Communications. *IEEE Access* **2019**, *7*, 149026–149038. [CrossRef]
20. Tuovinen, T.; Berg, M.; Yazdandoost, K.Y.; Iinatti, J. Ultra wideband loop antenna on contact with human body tissues. *IET Microwaves, Antennas Propag.* **2013**, *7*, 588–596. [CrossRef]
21. Zahran, S.R.; Abdalla, M.A.; Gaafar, A. New thin wide-band bracelet-like antenna with low SAR for on-arm WBAN applications. *IET Microw. Antennas Propag.* **2019**, *13*, 1219–1225. [CrossRef]
22. Shay, W.-T.; Jan, S.-C.; Tarng, J.H. A Reduced-Size Wide Slot Antenna for Enhancing Along-Body Radio Propagation in UWB On-Body Communications. *IEEE Trans. Antennas Propag.* **2013**, *62*, 1194–1203. [CrossRef]
23. Kissi, C.; Särestöniemi, M.; Kumpuniemi, T.; Myllymäki, S.; Sonkki, M.; Mäkelä, J.-P.; Nabil Srifi, M.; Jantunen, H.; Pomala-za-Raez, C. Receiving UWB antenna for wireless capsule endoscopy communications. *Prog. Electromagn. Res. C* **2020**, *101*, 53–69. [CrossRef]
24. Blauert, J.; Kiourti, A. Bio-Matched Horn: A Novel 1–9 GHz On-Body Antenna for Low-Loss Biomedical Telemetry with Implants. *IEEE Trans. Antennas Propag.* **2019**, *67*, 5054–5062. [CrossRef]
25. Shang, J.; Yu, Y. An Ultrawideband Capsule Antenna for Biomedical Applications. *IEEE Antennas Wirel. Propag. Lett.* **2019**, *18*, 2548–2551. [CrossRef]
26. Kirtania, S.G.; Elger, A.W.; Hasan, R.; Wisniewska, A.; Sekhar, K.; Karacolak, T.; Sekhar, P.K. Flexible Antennas: A Review. *Micromachines* **2020**, *11*, 847. [CrossRef] [PubMed]
27. Jahnavi, R.; Choudhary, A.; Singh, A.; Singh, V.; Bansal, P. Wearable and Flexible Wireless System Technology: A Review. In Proceedings of the 2019 6th International Conference on Computing for Sustainable Global Development (INDIACom), New Delhi, India, 13–15 March 2019; pp. 268–275.
28. Mohamadzade, B.; Hashmi, R.M.; Simorangkir, R.B.V.B.; Gharaei, R.; Ur Rehman, S.; Abbasi, Q.H. Recent Advances in Fab-rication Methods for Flexible Antennas in Wearable Devices: State of the Art. *Sensors* **2019**, *19*, 2312. [CrossRef] [PubMed]
29. Rao, M.V.; Madhav, B.T.P.; Anilkumar, T.; Prudhvinadh, B. Circularly polarized flexible antenna on liquid crystal polymer substrate material with metamaterial loading. *Microw. Opt. Technol. Lett.* **2020**, *62*, 866–874. [CrossRef]
30. Meredov, A.; Klionovski, K.; Shamim, A. Screen-Printed, Flexible, Parasitic Beam-Switching Millimeter-Wave Antenna Array for Wearable Applications. *IEEE Open J. Antennas Propag.* **2020**, *1*, 2–10. [CrossRef]
31. Mustafa, A.B.; Rajendran, T. An Effective Design of Wearable Antenna with Double Flexible Substrates and Defected Ground Structure for Healthcare Monitoring System. *J. Med. Syst.* **2019**, *43*, 186. [CrossRef]
32. Ullah, M.; Islam, M.; Alam, T.; Ashraf, F. Paper-Based Flexible Antenna for Wearable Telemedicine Applications at 2.4 GHz ISM Band. *Sensors* **2018**, *18*, 4214. [CrossRef]
33. Reddy, B.N.B.; Kumar, P.S.; Rao, T.R.; Tiwari, N.; Balachary, M. Design and Analysis of Wideband Monopole Antennas for Flexible/Wearable Wireless Device Applications. *Prog. Electromagn. Res. M* **2017**, *62*, 167–174. [CrossRef]
34. Shi, S.-R.; Wu, Y.-M.; Lu, P.-P.; Wu, Q. Investigation on the radiation features of the flexible antenna at 5.8 GHz. In Proceedings of the 2014 3rd Asia-Pacific Conference on Antennas and Propagation, Harbin, China, 26–29 July 2014; Institute of Electrical and Electronics Engineers (IEEE); pp. 1496–1500.
35. Rahman, M.A.; Hossain, M.F.; Riheen, M.A.; Sekhar, P.K. Early Brain Stroke Detection using Flexible Monopole Antenna. *Prog. Electromagn. Res. C* **2020**, *99*, 99–110. [CrossRef]
36. Alqadami, A.S.M.; Nguyen-Trong, N.; Mohammed, B.; Stancombe, A.E.; Heitzmann, M.T.; Abbosh, A. Compact Unidirectional Conformal Antenna Based on Flexible High-Permittivity Custom-Made Substrate for Wearable Wideband Electromagnetic Head Imaging System. *IEEE Trans. Antennas Propag.* **2020**, *68*, 183–194. [CrossRef]
37. Mohamadzade, B.; Simorangkir, R.B.V.B.; Hashmi, R.M.; Chao-Oger, Y.; Zhadobov, M.; Sauleau, R. A Conformal Band-Notched Ultrawideband Antenna with Monopole-Like Radiation Characteristics. *IEEE Antennas Wirel. Propag. Lett.* **2019**, *19*, 203–207. [CrossRef]
38. Simorangkir, R.B.V.B.; Kiourti, A.; Esselle, K. UWB Wearable Antenna with a Full Ground Plane Based on PDMS-Embedded Conductive Fabric. *IEEE Antennas Wirel. Propag. Lett.* **2018**, *17*, 493–496. [CrossRef]
39. Wang, Z.; Qin, L.; Chen, Q.; Yang, W.; Qu, H. Flexible UWB antenna fabricated on polyimide substrate by surface modification and in situ self-metallization technique. *Microelectron. Eng.* **2019**, *206*, 12–16. [CrossRef]
40. Abbasi, Q.H.; Rehman, M.U.; Yang, X.; Alomainy, A.; Qaraqe, K.; Serpedin, E. Ultrawideband Band-Notched Flexible Antenna for Wearable Applications. *IEEE Antennas Wirel. Propag. Lett.* **2013**, *12*, 1606–1609. [CrossRef]
41. Smida, A.; Iqbal, A.; Alazemi, A.J.; Waly, I.M.; Ghayoula, R.; Kim, S. Wideband Wearable Antenna for Biomedical Telemetry Applications. *IEEE Access* **2020**, *8*, 15687–15694. [CrossRef]
42. Hamouda, Z.; Wojkiewicz, J.; Pud, A.A.; Kone, L.; Bergheul, S.; Lasri, T. Flexible UWB organic antenna for wearable technologies application. *IET Microw. Antennas Propag.* **2018**, *12*, 160–166. [CrossRef]

43. Hamouda, Z.; Wojkiewicz, J.-L.; Pud, A.A.; Kone, L.; Bergheul, S.; Lasri, T. Magnetodielectric Nanocomposite Polymer-Based Dual-Band Flexible Antenna for Wearable Applications. *IEEE Trans. Antennas Propag.* **2018**, *66*, 3271–3277. [CrossRef]
44. Saeed, S.M.; Balanis, C.A.; Birtcher, C.R.; Durgun, A.; Shaman, H.N. Wearable Flexible Reconfigurable Antenna Integrated with Artificial Magnetic Conductor. *IEEE Antennas Wirel. Propag. Lett.* **2017**, *16*, 2396–2399. [CrossRef]
45. Ashyap, A.Y.I.; Bin Dahlan, S.H.; Abidin, Z.Z.; Abbasi, M.I.; Kamarudin, M.R.; Majid, H.A.; Dahri, M.H.; Jamaluddin, M.H.; Alomainy, A. An Overview of Electromagnetic Band-Gap Integrated Wearable Antennas. *IEEE Access* **2020**, *8*, 7641–7658. [CrossRef]
46. Arif, A.; Zubair, M.; Ali, M.; Khan, M.U.; Mehmood, M.Q. A Compact, Low-Profile Fractal Antenna for Wearable On-Body WBAN Applications. *IEEE Antennas Wirel. Propag. Lett.* **2019**, *18*, 981–985. [CrossRef]
47. Gao, G.; Hu, B.; Wang, S.; Yang, C. Wearable Circular Ring Slot Antenna With EBG Structure for Wireless Body Area Network. *IEEE Antennas Wirel. Propag. Lett.* **2018**, *17*, 434–437. [CrossRef]
48. Liu, X.Y.; Di, Y.H.; Liu, H.; Wu, Z.T.; Tentzeris, M.M. A Planar Windmill-like Broadband Antenna Equipped with Artificial Magnetic Conductor for Off-Body Communications. *IEEE Antennas Wirel. Propag. Lett.* **2015**, *15*, 64–67. [CrossRef]
49. Abirami, B.S.; Sundarsingh, E. EBG-Backed Flexible Printed Yagi–Uda Antenna for On-Body Communication. *IEEE Trans. Antennas Propag.* **2017**, *65*, 3762–3765. [CrossRef]
50. Biswas, A.; Islam, A.J.; Al-Faruk, A.; Alam, S.S. Design and performance analysis of a microstrip line-fed on-body matched flexible UWB antenna for biomedical applications. In Proceedings of the 2017 International Conference on Electrical, Computer and Communication Engineering (ECCE), Cox's Bazar, Bangladesh, 16–18 February 2017; pp. 181–185.
51. Xiao, W.; Mei, T.; Lan, Y.; Wu, Y.; Xu, R.; Xu, Y. Triple band-notched UWB monopole antenna on ultra-thin liquid crystal polymer based on ESCSRR. *Electron. Lett.* **2017**, *53*, 57–58. [CrossRef]
52. Zhang, H.; Li, H. Flexible Dual-polarized UWB Antennas for Breast Tumor Imaging. In Proceedings of the 2020 IEEE MTT-S International Conference on Numerical Electromagnetic and Multiphysics Modeling and Optimization (NEMO), Hangzhou, China, 7–9 December 2020; pp. 1–2.
53. Rahayu, Y.; Saputra, R. Design Strategy on Medical Wearable Antenna for Tumor Detection. In Proceedings of the 2020 International Symposium on Antennas and Propagation (ISAP), Osaka, Japan, 25–28 January 2021; pp. 105–106.
54. Awan, W.A.; Naqvi, S.I.; Hussain, N.; Ghaffar, A.; Zaidi, A.; Li, X.J. A Miniaturized UWB Antenna for Flexible Electronics. In Proceedings of the 2020 IEEE International Symposium on Antennas and Propagation and North American Radio Science Meeting, Montréal, QC, Canada, 5–10 July 2020; Institute of Electrical and Electronics Engineers (IEEE); pp. 99–100.
55. CST Microwave Studio. Available online: http://www.cst.com. (accessed on 1 June 2020).
56. Orfanidis, S.J. Electromagnetic Waves and Antennas. 2002. Available online: http://www.ece.rutgers.edu/~{}orfanidi/ewa/ (accessed on 2 January 2020).
57. Available online: https://www.itis.ethz.ch/virtual-population/tissueproperties/database/dielectric-properties/ (accessed on 2 January 2020).
58. Sarestoniemi, M.; Kissi, C.; Raez, C.P.; Hamalainen, M.; Iinatti, J. Impact of the Antenna-Body Distance on the WBAN Channel Characteristics. In Proceedings of the 2019 13th International Symposium on Medical Information and Communication Technology (ISMICT), Oslo, Norway, 8–10 May 2019; pp. 1–6. [CrossRef]
59. Sarestoniemi, M.; Pomalaza-Raez, C.; Kissi, C.; Iinatti, J. Simulation and Measurement Data-Based Study on Fat as Propagation Medium in WBAN Abdominal Implant Communication Systems. *IEEE Access* **2021**, *9*, 46240–46259. [CrossRef]
60. Sarestoniemi, M.; Pomalaza-Raez, C.; Sayrafian, K.; Iinatti, J. In-Body Propagation at ISM and UWB Frequencies for Abdominal Monitoring Applications. In Proceedings of the 2021 IEEE International Conference on Communications Workshops (ICC Workshops), Vancouver, BC, Canada, 14–23 June 2021; Institute of Electrical and Electronics Engineers (IEEE); pp. 1–5.
61. Vauche, R.; Muhr, E.; Fourquin, O.; Bourdel, S.; Gaubert, J.; Dehaese, N.; Meillere, S.; Barthelemy, H.; Ouvry, L. A 100 MHz PRF IR-UWB CMOS Transceiver with Pulse Shaping Capabilities and Peak Voltage Detector. *IEEE Trans. Circuits Syst. I Regul. Pap.* **2017**, *64*, 1612–1625. [CrossRef]
62. Ha, J.O.; Jung, S.H.; Park, M.C.; Lee, K.H.; Eo, Y.S. A fully integrated 3–5 GHz UWB RF transceiver for WBAN applications. In Proceedings of the 2013 IEEE MTT-S International Microwave Workshop Series on RF and Wireless Technologies for Biomedical and Healthcare Applications (IMWS-BIO), Singapore, 9–11 December 2013; pp. 1–3. [CrossRef]